Amelioration of Convective and Nonconvective Condensation with the Assimilation of Rainfall for Improving Initial Conditions

MUKUT B. MATHUR

National Meteorological Center, Development Division, Washington, D.C.

(Manuscript received 24 June 1994, in final form 4 November 1994)

ABSTRACT

Three new schemes to assimilate the rainfall observations for improving the initial conditions are developed and tested. A reverse cumulus parameterization procedure is used in which the model convective precipitation is nudged in scheme 1, and the model total precipitation is nudged in schemes 2 and 3, toward the observations. At the nonconvective grid points, the reverse procedure is not invoked. A method to enhance the rainfall at such points, in case the predicted total rainfall is weaker than the observed, is included in scheme 3. Numerical results are presented to show that the thermodynamic and wind fields and the distribution of condensational heating are improved with the use of any of the above rainfall assimilation schemes. The incorporation of the method to enhance the rainfall at the nonconvective grid points and the use of the total rainfall in place of only the convective rainfall in the reverse procedure ameliorate the initial conditions.

1. Introduction

Low-latitude disturbances, like tropical storms, often develop over oceanic regions. Air at low levels in these circulations flows toward the center, picking up moisture and sensible heat. Release of latent heat mostly in the form of convective clouds occurs as the inflowing air moves upward. This condensational heating is a dominant source of energy for these disturbances. Strong outflow develops in the upper troposphere as these circulations intensify. Poleward transport of heat in outflow layers often affects high-latitude currents. Thus, a realistic prognosis of diabatic effects in tropical areas can lead to the enhancement of the structure and intensity of both low- and midlatitude circulations in a numerical model.

Because of a lack of observations over tropical oceans, the moisture and divergence fields are often not well analyzed, and the diabatic forcing of the tropical atmosphere is not well predicted in numerical models. Forecast rainfall amounts and storm intensity are often weaker than those derived from available conventional and satellite measurements. On the other hand, initial analysis errors in some cases produce a stronger than observed storm intensity and precipitation amounts.

For improving initial conditions in tropical regions, Mathur et al. (1992) used a reverse convective parameterization scheme in the global Medium-Range Forecast Model (MRF) of the National Meteorological Center (NMC). The convective precipitation in the MRF between 30°N and 30°S was nudged toward the observed rainfall amounts for a 24-h interval (initialization period) prior to a forecast. Because the conventional rainfall observations are sparse over tropical regions, rainfall amounts derived from satellite measurements of OLR (outward-going longwave radiation) were used as observations. A reverse Kuo scheme, based on Krishnamurti et al. (1988, 1990), was used during the initialization. Forecasts were carried out with and without the use of the initialization procedure. The forecast fields were superior in the initialized than in the uninitialized case.

The reverse Kuo scheme was also used in NMC's Global Data Assimilation System (GDAS) for the ingestion of the rainfall data by Mathur et al. (1992). The analysis in GDAS is carried out at 6-h intervals. The 6-h MRF forecast from the analysis of the previous cycle of GDAS is used as a first guess for the next analysis. Assimilation to 96 h was carried out with (OLR GDAS) and without (CONTROL GDAS) the use of the reverse Kuo in the forecast cycle of GDAS. The analyzed circulation at 96 h was superior in OLR GDAS than in CONTROL GDAS. A 120-h forecast (without reverse Kuo) was carried out in both cases starting with the analysis at 96 h. The forecast circulations from the OLR GDAS analysis were better than those with the CONTROL GDAS analysis. Reverse cumulus schemes also have been used in other previous studies (Donner 1988; Puri and Miller 1990; Kasahara et al. 1992).

In the Mathur et al. (1992) scheme, the model convective cloud sounding is calculated twice at the grid

Corresponding author address: Dr. Mukut B. Mathur, Development Division, W/NMC22:MBM, National Meteorological Center, Washington, DC 20233.

points where the rainfall adjustment is carried out. The computational time for a model run is therefore greater with the use of the nudging scheme. Also, the model convective precipitation (and not the total precipitation) was nudged toward the observations in the above scheme. Excessive rainfall was produced at the grid points where, in addition to the adjustment of the convective rain toward the observed rainfall, the nonconvective precipitation also occurred. Furthermore, the model precipitation was nudged toward the observations only at the grid points where the model produced convective rain. Thus, no adjustment was made at the grid points where convection was not predicted in the model, even though the rainfall was observed at these grid points. Another difficulty in the above study arose due to the availability of the OLR rainfall rates at only 24-h intervals, while the precipitation over small areas in association with tropical disturbances is known to often last only for a few hours. This shortfall in observations was partially compensated for by adjusting the OLR rainfall rate every six hours in each 24-h period. As an example, if no model rainfall occurred at a grid point in the first 18 h of a 24-h period, then the OLR rainfall rate was increased four times at this grid point for the 18–24-h interval. This adjustment of the observed rate did not improve the results in areas where the rainfall mainly occurred in the first 6-h period (the nudging procedure will try to adjust the model rain to the one-fourth of the 24-h observed amount), but it led to a considerable improvement in areas where the rain mainly occurred in the last 6 h of a 24-h period.

A main purpose of this study is to develop and test new schemes to overcome above cited deficiencies in the rainfall initialization procedure. We have developed and tested three new schemes. The nudging procedure in new schemes is based on Krishnamurti et al. (1988, 1990) and Mathur et al. (1992). The new schemes are more efficient computationally because the convective sounding is evaluated only once at each time step instead of twice per time step as in the Mathur et al. (1992) scheme. In the reverse Kuo procedure, the convective precipitation during a time step is nudged toward the observed values in the first scheme. The total model precipitation is adjusted toward the observations in the second and the third scheme. The adjustment of total rain is carried out by evaluating the difference between the model total rainfall and the observed total rainfall and then nudging the model convective rainfall toward this difference. Our motivation for nudging total model rainfall, in place of only the convective rainfall, is discussed in section 3b. A procedure to increase the rainfall at the nonconvective grid points, when the observed rainfall is greater than the model rainfall, is included in the third scheme. Recall that no adjustment is made at such grid points in the Mathur et al. (1992) scheme. It was noted above that it would be advantageous to have the rainfall data at intervals that are shorter than 24 h. In this regard, efforts are underway at the NMC to produce the rainfall estimates at 6-h intervals over Tropics between 30°N and 30°S from the geostationary satellite data. Because the above satellite-derived rainfall data at short intervals over the entire tropical area are not yet available, the new schemes have not been tested using GDAS and MRF.

In the present study, we have used a regional (tropical storm) model, the NMC's Quasi-Lagrangian Model (QLM), to test the performance of the new schemes. An overview of the QLM is provided in section 2. A description of the new schemes is given in section 3. The design of experiments and numerical results are discussed in section 4. Previous studies have indicated that numerical models do not produce initial realistic precipitation, partly because the moisture field is not well analyzed due to a lack of observations. The relative humidity (RH) in the storm area is specified in the QLM. The impact of lowering initial RH in the storm area (inserts moisture deficiency) and results from nudging of rainfall produced from such an initial state toward the rainfall produced in the QLM with the use of a higher initial value of RH (normal specification) are discussed. Our conclusions are presented in section 5.

2. The QLM

The primitive equations with σ (pressure/surface pressure) as the vertical coordinate are integrated using a quasi-Lagrangian scheme. A grid spacing of 40 km over a 4400 km × 4400 km area and 16 layers are used in this study. The variables are not staggered in the horizontal. The vertical velocity is defined at the interfaces between the layers and it vanishes at the top and bottom of the model atmosphere. All other variables are defined in the layers. The values of σ at the interfaces are 1.0, 0.965, 0.922, 0.872, 0.816, 0.754, 0.688, 0.618, 0.546, 0.472, 0.397, 0.328, 0.250, 0.181, 0.114, 0.054, and 0.0.

a. Condensational processes

Both nonconvective (large scale) and convective release of latent heats are included in the QLM. The nonconvective heating is only invoked at the supersaturated grid points; both the temperature and moisture at such points are modified so that the adjusted state has 100% relative humidity. The convective parameterization scheme is based on Kuo (1965). The fractional area a_0 covered by the newly formed clouds at a grid point in a time step is given by

$$a_0 = \frac{I}{Q}, \tag{1}$$

where I is the moisture available in a time step to produce convective clouds and Q is the moisture needed to saturate the grid column with convective clouds between the base and top of the cloud. An expression for

Q is given below. In the operational version of the QLM for hurricane prediction, the moisture available I is taken as the vertical moisture flux in the layer from which the cloud parcel originates. The increase in moisture between the base and top of the cloud in a time step due to processes other than condensational defines I in the MRF (Mathur et al. 1992). This last definition of I is used in the QLM integrations presented in this paper to make the procedure for the evaluation of I in the QLM similar to the one used in the MRF.

The rate of heating H and the rate of increase of moisture M at a level p may be written as

$$H(p) = a_0 c_p[T_c(p) - T(p)], \tag{2}$$

and

$$M(p) = a_0[q_c(p) - q(p)]. \tag{3}$$

Here c_p is the specific heat of air at constant pressure, and T and q are, respectively, the temperature and specific humidity at a grid point before the convective condensation is evaluated. A subscript c on a variable denotes the value of the variable within the model convective cloud. In the present study, the convective cloud is given by the (moist adiabatic) ascent through the lifting condensation level of the parcel from the lowest model layer. With this definition of a convective cloud, Q is given by

$$Q = \frac{c_p}{L}\int [T_c(p) - T(p)]dp + \int [q_c(p) - q(p)]dp. \tag{4}$$

The convective rainfall is given by

$$P_c = \frac{1}{gL}\int H(p)dp. \tag{5}$$

b. *Initial data*

The procedure used in the operational version of the QLM for the prediction of (tropical) storm tracks is utilized to define the initial state. The initial analysis on the QLM grid is obtained by interpolation of NMC's global aviation analysis. An idealized vortex whose size and intensity match those of the observed storm is constructed. The winds in this vortex are cyclonic at low levels, with the maximum wind close to the vortex center. The cyclonic winds decrease first slowly and then rapidly with height, and anticyclonic winds appear in the high troposphere. The height field is developed based on the gradient wind relation. The virtual temperature is derived using the hydrostatic equation. The relative humidity in the idealized vortex is specified, and the RH values depend on the intensity of the storm. Based on the current storm motion, a steering current is imposed on the vortex. The combined circulation (vortex plus steering current) is then merged into the QLM gridded analysis. A complete description of the QLM, including its initialization procedure, is provided in Mathur (1991).

3. Rainfall assimilation procedures

a. *Scheme 1: Adjustment of the convective rain toward the observed rain*

Precipitation observations are generally available at some constant time intervals. Let P_o denote the target (or observed) rainfall during a time step Δt. In the present and in the earlier study (Mathur et al. 1992), P_o is calculated from the mean rainfall rate during the interval for which rainfall amounts were available. We evaluated P_o and initialized the forecast precipitation to zero at the beginning of each interval.

The adjustment process consists of two steps. In the first step, we calculate (T_c, q_c) and then P_c from (5) using (1)–(4). In the second step, we adjust P_c toward P_o, but only at grid points where $P_c > 0$. For this purpose we define β_1 and a_1 as

$$\beta_1 = \frac{P_o}{P_c}, \tag{6}$$

and

$$a_1 = \beta_1 a_0. \tag{7}$$

If we replace a_0 by a_1 in the evaluation of $H(p)$ and $M(p)$ from (2) and (3), respectively, and then calculate P_c from (5), the new value of P_c will be equal to P_o. Thus, a_1 is construed as the fractional cloud cover needed so that P_c equals P_o. However, because of the following restrictions on a_1 and β_1, the forecast rainfall is not exactly adjusted to the observed. We envision that as a result of convection, (T, q) in a vertical column can at most attain the values equal to those in the model cloud (T_c, q_c). This implies that a_1 cannot exceed unity. In our tests we did not allow a_1 to exceed 0.99. Furthermore, significant amounts of rainfall often occur in association with cyclonic disturbances, and the location of a predicted storm may differ from its observed position. Because of this phase error, the forecast area of rainfall is likely to be displaced from the observed rainfall area. In such a case, if we adjust the rainfall to zero in a time step at grid points where the rainfall is predicted but not observed, the model storm may dissipate. We therefore set a lower limit β^* for β_1. We used $\beta^* = 0.5$ in our experiments; a value for β^* much lower than 0.5 may be considered undesirable because then, as noted above, a disturbance whose location is not well predicted may dissipate. However, for a tropical storm case discussed in section 4, the differences between two integrations, one using $\beta^* = 0.5$ and the other $\beta^* = 0.1$, were small.

In the application of the above scheme, we first calculated a_0 and P_c using (1)–(5), and then evaluated

β_1 from (6). After imposing the condition $\beta_1 \geq \beta^*$, a_1 was calculated from (7). We set $a_1 = 0.99$ if it was greater than 0.99. We replaced a_0 by a_1 in (2) and (3) to evaluate the adjusted (nudged) heating and moistening rates and then computed the convective precipitation from (5).

b. *Scheme 2: Inclusion of the total rainfall in the reverse procedure*

A few observational studies have suggested that nearly 40% of rain in tropical precipitating systems does not fall from the convective clouds (e.g., see Cheng and Houze 1979). Also, procedures have been recently developed to estimate both tropical convective and nonconvective precipitation from satellite data (Adler and Negri 1988). Synoptic and other surface observations of total rainfall can be included in data used for rainfall analysis. Thus, utilization of all available observations will give an estimate of total rainfall. In a numerical model like the QLM or the MRF, the convective precipitation is evaluated using a parameterization procedure. In a recent integrations of the QLM, a grid spacing of 20 km was used and both nonconvective and parameterized convective heating rates were saved. In vertical columns near the predicted hurricane center, large upward motion was simulated and the nonconvective heating was much greater than the parameterized convective heating in these columns. Mathur and Baldwin (1994) integrated the eta model of the NMC using a grid spacing of 80 km in a blizzard of 1993 case. This storm occurred over the eastern United States, and the initial rapid intensification (about 25 mb fall in mean sea level pressure during the first 24 h) was associated with the condensational heating. Vertical columns near the storm center with large upward motion and strong nonconvective heating were simulated. The parameterized convective heating was very weak or absent. Thus, the heating on the convective scale in the two numerical integrations cited above is simulated as the nonconvective heating. Considering the above model results and likelihood that observations will give us an estimate of total rainfall, we developed a nudging scheme in which the model total precipitation is adjusted toward the observed rainfall.

The large-scale release of latent heat in the QLM is evaluated at the grid points where the relative humidity exceeds 100%. This heating is calculated at the beginning of a time step and then the convective heating is computed. Let P_{ls} denote the large-scale rainfall at a grid point during a time step. As in scheme 1, we first calculate P_c from (5) using (1)–(4). In the second step, we adjust the total model rainfall toward the observed rainfall, but only at grid points where $P_c > 0$. For this purpose we set a_2 as

$$a_2 = \beta_2 a_0. \tag{8}$$

We defined β_2 in two ways:

$$\beta_2 = \frac{P_o - P_{ls}}{P_c}, \tag{9}$$

and

$$\beta_2 = \frac{P_o T - P_m \Delta t}{P_c \Delta t}. \tag{10}$$

Here T is the time since the forecast precipitation was last initialized to zero, and P_m is the total model precipitation up to the current time step plus the nonconvective precipitation (P_{ls}) that has occurred in the current time step. Note that the convective precipitation that occurs in the current time step is not included in P_m.

In (9), $\beta_2 P_c$ is the convective rainfall that is required so that the sum of the large-scale (P_{ls}) and convective ($\beta_2 P_c$) rainfalls equals the observed precipitation (P_o) during a time step, while $\beta_2 P_c$ in (10) is the convective precipitation required so that ($\beta_2 P_c + P_m$) equals the observed rainfall up to the current time step. For nudging the total (model) rainfall toward the observed rainfall, the convective precipitation in a time step is evaluated in (10) from the difference between the observed and the forecast precipitation amounts up to the current time step, while it is calculated in (9) from the difference between the observed and the large-scale (model) rainfall amounts in the current time step.

We impose the conditions $\beta_2 \geq 0.5$ and $a_2 \leq 0.99$. The above conditions on (β_2, a_2) are similar to those imposed on (β_1, a_1) in scheme 1. We replace a_0 by a_2 in the evaluation of $H(p)$ and $M(p)$ from (2) and (3), respectively, and then obtain the adjusted convective precipitation from (5). Because of the restrictions on (β_2, a_2) cited above, the total precipitation, with the use of a_2 in the evaluation of convective rainfall, may not equal the observed precipitation.

Manobianco et al. (1994) also nudged total model rainfall toward observations in a case study. Our procedure, however, is very different from one used in Manobianco et al. As an example, only temperature is adjusted in the rainfall assimilation scheme of Manobianco et al. (moisture is also adjusted only in case the model precipitation is less than one-half the observed precipitation). On the other hand, both moisture and temperature are adjusted whenever our scheme is invoked.

c. *Scheme 3: Adjustment of the rainfall in nonconvective regions*

In schemes 1 and 2 described above, the forecast precipitation is nudged toward the observed rainfall only at the grid points where the convective rainfall is predicted. The rainfall adjustment also was carried out only at convective points in the Mathur et al. (1992) study. We describe below a simple procedure for nudg-

ing the rainfall at the nonconvective grid points when the model rainfall is less than the observed rainfall. The nudging of the precipitation at such grid points when the model rainfall is greater than the observed rainfall will be attempted in future studies.

We define Υ as the difference between the observed and forecast rainfall up to the current time step:

$$\Upsilon = P_o \frac{T}{\Delta t} - P_m.$$

The NMC uses inch as the unit for rainfall, and this unit is employed in our study in place of the standard unit meter. A critical value Υ_{ck} is prescribed for each model layer. In this preliminary approach, we increase the mixing ratio to its saturated value in the layers for which $\Upsilon_{ck} \leq \Upsilon$, but only if no convective rain was produced in the previous time step. The numerical results for the case discussed in section 4 depended on Υ_{ck}. Best results were obtained with Υ_{ck} selected so that we saturated layers 8–10 for $0 < \Upsilon < 1$, layers 7–11 for $1 < \Upsilon < 2$, layers 6–12 for $2 < \Upsilon < 3$, layers 5–13 for $3 < \Upsilon < 4$, and layers 4–14 for $\Upsilon > 4$. Note that for the values of σ at interfaces used in this study (section 2) and the surface pressure near 1000 mb, layer 4 would be near 850 mb, layer 9 near 500 mb, and layer 13 near 200 mb. In the real atmosphere the stratiform rain often first develops in the midtroposphere; therefore, for small values of Υ (<1), we saturate three midtropospheric layers. More layers are saturated for a larger value of Υ. We envision that supersaturation in the subsequent time steps may occur in the layers that are saturated as a result of the above procedure, and the ensuing condensation will produce rainfall. With the application of this scheme, the forecast rainfall may be expected to increase in the outer area of a storm where weak upward vertical motion but unsaturated air may be predicted in a numerical forecast; see section 4b for an example.

4. Numerical results

a. Design of experiments

The QLM was integrated for 24 h using the data for 0000 UTC 17 September 1991. At this initial time, Bob was a tropical storm and it developed into a hurricane during the next 24 h. A list of experiments discussed in this section is provided in Table 1. According to the operational procedure used in the QLM (Mathur 1991), the RH values in low levels were specified to be greater than 90% in the idealized vortex with maximum values near the storm center. The initial state with the above values of RH will be referred to as the RH90 initial state.

Because of lack of data in tropical regions, the moisture and divergence fields are not often well analyzed. This deficiency in analysis leads to a slow spinup of model physics and underprediction of rainfall amounts.

TABLE 1. List of experiments.

Experiment	Initial relative humidity in the vortex	Nudging procedure
RH90	>90%	—
RH80	>80%	—
RH80C	>80%	Convective precipitation in the reverse Kuo scheme (scheme 1)
RH80T	>80%	Total precipitation in the reverse Kuo scheme (scheme 2)
RH80TL	>80%	Total precipitation in the reverse Kuo scheme—saturation of a part of the vertical column at points where the convective rain is not predicted (scheme 3)

In this paper we consider a model atmosphere that is represented by the 24-h QLM forecast from the RH90 initial state. This model atmosphere is also referred to as the RH90 forecast. Then we consider another initial state (referred to as the RH80 initial state) that is the same as the RH90 initial state, except that the relative humidity over the storm area is lower in the RH80 initial state than in the RH90 initial state. Thus, the RH80 initial state is intended to represent a case where the deficiency in the initial state is in the moisture field. We integrated the QLM from the RH80 initial state (results of integration are referred to as the RH80 forecast) and found that forecast storm intensity and rainfall were much weaker in the RH80 forecast (weak spinup) than in the RH90 forecast.

The total precipitation in RH90 was saved for each 6-h interval. Three additional experiments were carried out starting with the RH80 initial state and nudging the forecast rainfall toward the RH90 precipitation values cited above. The convective precipitation was nudged (scheme 1) in the experiment RH80C, while the total precipitation was nudged (scheme 2) in the experiment RH80T. The nudged solution at 24 h was better with the use of (10) than (9) in scheme 2; the numerical results using (10) are discussed below in this section. Scheme 3 was used in the third experiment RH80TL. Forecast fields over only the storm area are shown in figures discussed in this section, and the predicted storm center is located close to the center of the area shown.

We have employed synthetic data (rainfall data produced in a model run, namely RH90) in place of observed data for testing our schemes. Use of synthetic data in testing a scheme has some advantages over utilizing the real data. It is well known that the structure of tropical disturbances depends on the vertical distribution of latent heating. The vertical distribution of latent heating is not obtained from the satellite data that are currently used to derive rainfall estimates. Distribution of heating is also not available from conven-

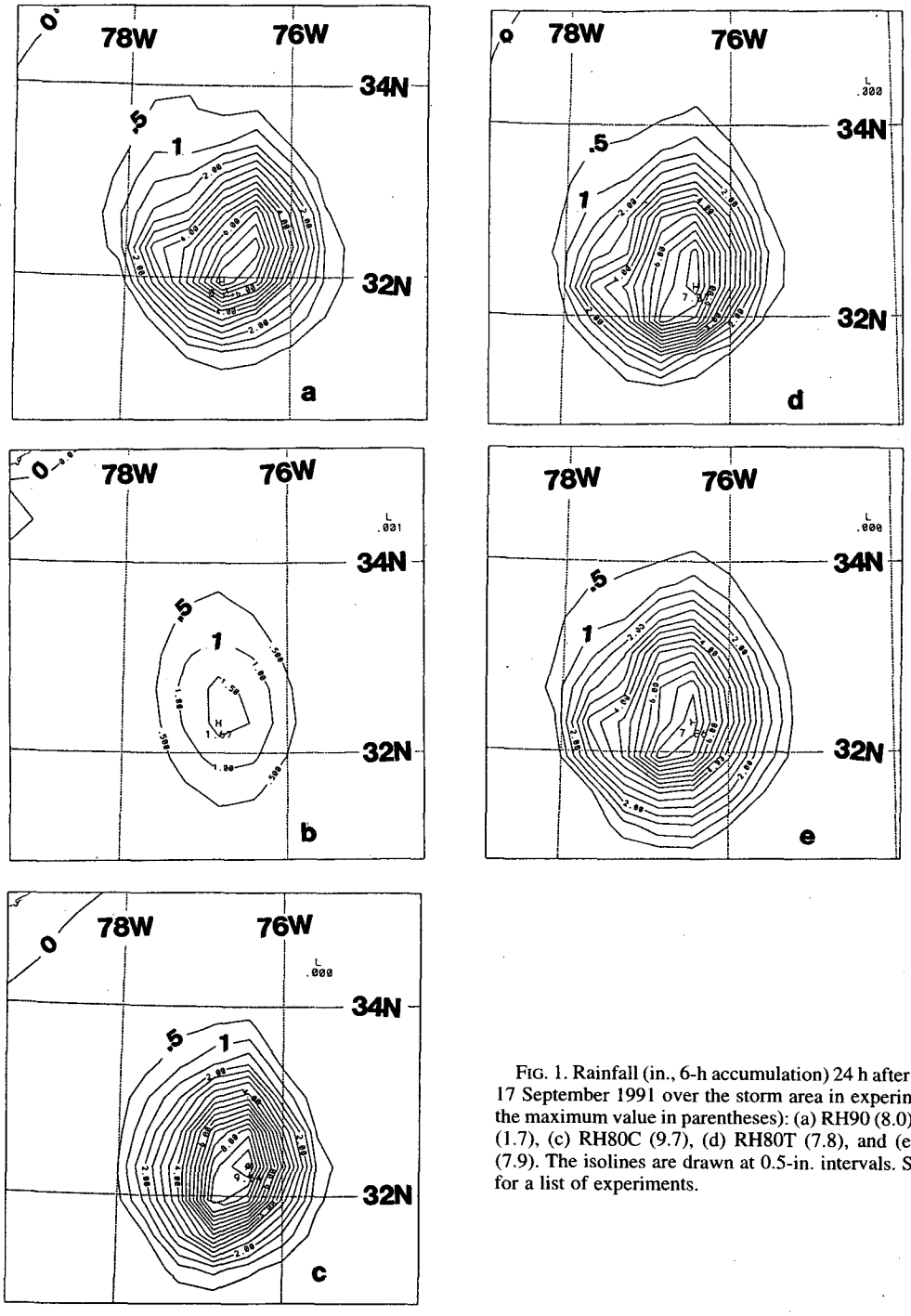

FIG. 1. Rainfall (in., 6-h accumulation) 24 h after 0000 UTC 17 September 1991 over the storm area in experiments (with the maximum value in parentheses): (a) RH90 (8.0), (b) RH80 (1.7), (c) RH80C (9.7), (d) RH80T (7.8), and (e) RH80TL (7.9). The isolines are drawn at 0.5-in. intervals. See Table 1 for a list of experiments.

tional data, and therefore the horizontal structure of latent heating at different levels cannot also be obtained from available observations. Because of the above deficiency in observations, one cannot infer the accuracy of vertical and horizontal distribution of latent heating produced in a model that uses observed rainfall data in a nudging procedure. On the other hand, the vertical and horizontal distribution of latent heating in a synthetic dataset, such as one used in our study (RH90 forecasts), is known. Therefore we can diagnose relative performance of rainfall assimilation schemes better (by comparing heating rates) with the use of synthetic

TABLE 2. Threat scores and bias.

Rainfall range (in.)	Threat scores				Bias			
	RH80	RH80C	RH80T	RH80TL	RH80	RH80C	RH80T	RH80TL
0.1–1.0	0.35	0.56	0.63	0.52	1.08	0.65	1.11	1.22
1.0–2.0	0.00	0.50	0.14	0.25	1.29	1.14	1.29	1.14
2.0–3.0	0.00	0.25	0.30	0.27	0.00	0.43	0.86	1.00
3.0–4.0	0.00	0.14	0.14	0.25	0.00	1.00	1.00	1.00
4.0–5.0	0.00	0.33	0.40	0.40	0.00	1.67	1.33	1.33
5.0–6.0	0.00	0.00	0.00	0.00	0.00	0.00	1.00	2.00
6.0–7.0	0.00	0.00	0.50	0.50	0.00	0.33	1.00	1.00
7.0–8.0	0.00	0.00	0.33	0.33	0.00	1.00	3.00	3.00

data (see section 4c). Other advantages of using synthetic data are given in Donner and Rasch (1989).

b. *Assimilated rainfall*

The 6-h accumulated rainfall amounts at 24 h in the five experiments listed in Table 1 are shown in Fig. 1. Clearly, the use of a lower initial relative humidity (experiment RH80) leads to a considerable reduction in the forecast rainfall (compare Figs. 1a and 1b). Both the area of rainfall and the maximum amount increase with the use of scheme 1 (experiment RH80C) in which the convective rainfall is nudged toward the RH90 precipitation (Fig. 1c). The lowest contour (0.5 in.) in Fig. 1c nearly coincides with the corresponding contour in Fig. 1a, except to the west and northwest of the center. However, the maximum value in RH80C (9.7 in.) is much greater than in RH90 (8 in.).

Both the structure (compare 4-in. isoline in Figs. 1a, 1c, and 1d) and the maximum value approach those in RH90, when scheme 2 is used (experiment RH80T). Recall that the total precipitation is nudged toward the RH90 values in scheme 2. Compared to RH80C, the lowest contour in RH80T is closer (farther) to the corresponding RH90 contour in the area to the west and northwest (north and southeast) of the center.

As noted in section 3, in addition to the nudging of the total precipitation during the (reverse) convective parameterization, a procedure to enhance the rainfall at nonconvective grid points is also included in scheme 3. This scheme is used in RH80TL. Among the three nudging experiments, the shape and area of the lowest contour (0.5 in.) are produced best in RH80TL (Fig. 1e); except to the north of the center, the lowest contour in RH80TL nearly coincides with that in RH90. The maximum contour (7.5 in.) in RH80TL also nearly coincides with the corresponding contour in RH90. The 7.5-in. contour in RH80T is located somewhat to the northwest of its location in RH90, and it occupies a much larger area in RH80C. Thus, both the rainfall area and amounts appear to be closer to the RH90 values in RH80TL than in RH80C and RH80T.

Threat score T and bias B are often used to measure the performance of a model's rainfall forecast. These two scores in RH80, RH80C, RH80T, and RH80TL were evaluated using the following:

$$T = \frac{H}{F + O - H},$$

and

$$B = \frac{F}{O}.$$

Here O and F are the number of observed and forecast points, respectively, that have precipitation amounts within a specified range, and H is the number of common points between O and F. A threat score of 1 implies that the rainfall points are equal in number and are the same in the forecast and observations. A bias of 1 indicates that the number of points in the forecast and observations is the same, and values greater (less) than 1 imply that the number of points in forecast is larger (smaller) than in observations. Note that in our study, O points are calculated from data in the experiment RH90 and F points from data in either RH80, RH80C, RH80T, or RH80TL.

The maximum rainfall in RH80 was less than 2 in., and the precipitation greater than 1 in. occurred in RH80 in the area where rainfall exceeding 3 in. was produced in RH90 (Fig. 1). Therefore, the threat scores for values over 1 in. are zero in RH80, and the bias is zero for values over 2 in. (Table 2). The threat scores in RH80C, RH80T, and RH80TL are larger than in RH80 in all ranges of precipitation. The bias is closer to 1 in RH80 than in other three experiments, only in the 0.1–1-in. range. Therefore, use of any of the three schemes improves the simulation of rainfall.

Threat scores in the 0.1–1- and 2–3-in. ranges are somewhat higher in RH80T than in RH80TL, while these are somewhat lower in the 1–2- and 3–4-in. ranges in RH80T than in RH80TL (Table 2). Threat scores for rainfall exceeding 4 in. are the same in RH80T and RH80TL. On the other hand, the threat scores for values exceeding 4 in. are smaller in RH80C than in RH80T or RH80TL, except that they are the same in the 5–6-in. range in all experiments. Threat score in RH80C is higher than in RH80T only in the

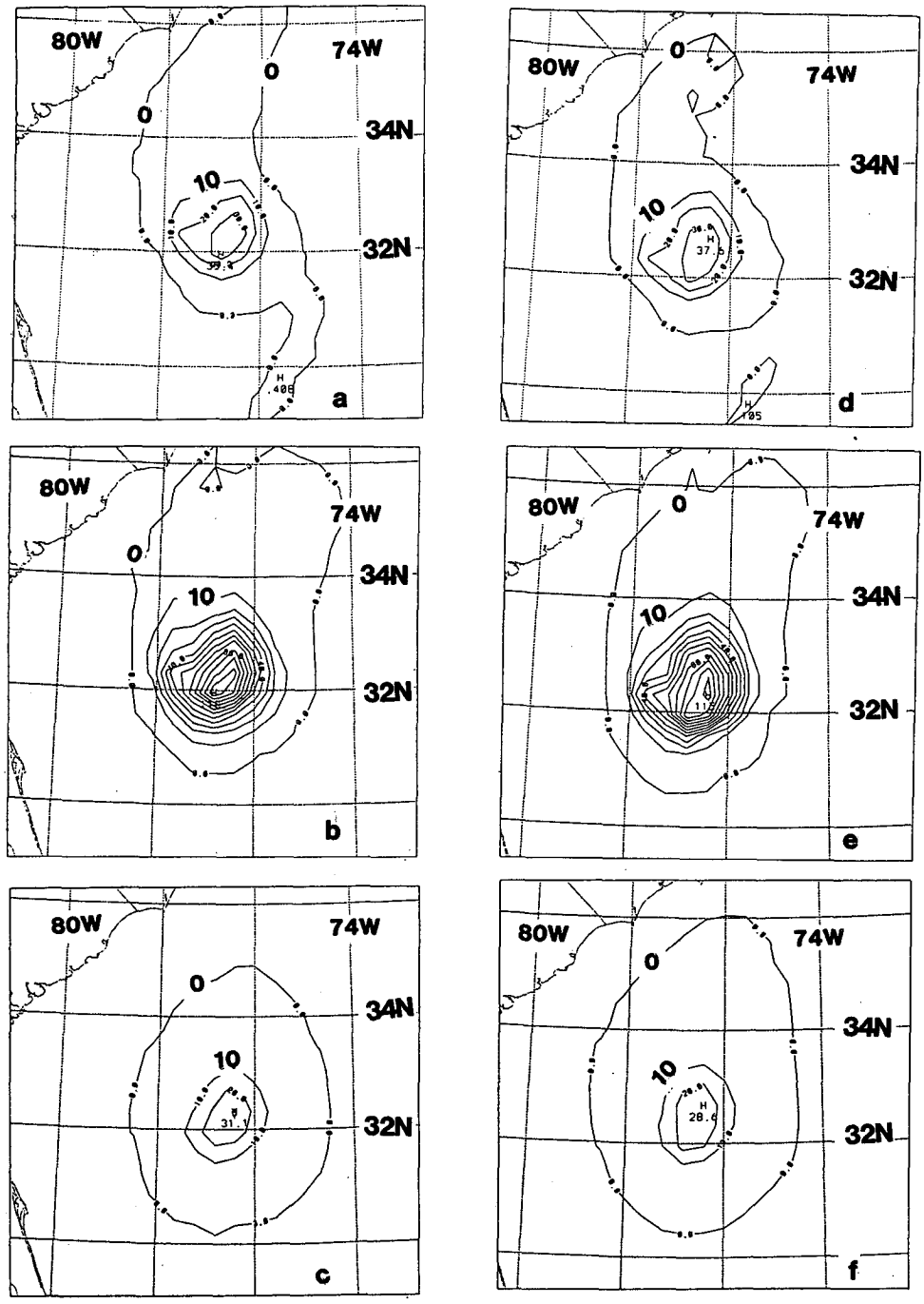

FIG. 2. Total (sum of convective and nonconvective) condensational release of latent heat 24 h after 0000 UTC 17 September 1991 over the storm area in experiments (with maximum value in parentheses): (a) RH90 at 850 mb (35), (b) RH90 at 500 mb (118), (c) RH90 at 200 mb (31), (d) RH80T at 850 mb (38), (e) RH80T at 500 mb (115), (f) RH80T at 200 mb (29). The isolines are drawn at 10 K (6 h)$^{-1}$ intervals. See Table 1 for a list of experiments.

1–2-in. range. Threat scores are larger in RH80C than in RH80TL only in ranges below 2 in. Considering the threat scores, RH80T performs much better than RH80C, and RH80TL scores are similar to RH80T.

A comparison of bias values shows that more points with some precipitation were predicted in RH80TL than in RH80C or RH80T. The number of points with rainfall between 1 and 8 in. was closer in RH90 (26)

TABLE 3. Maximum in total latent heating [K (6 h)$^{-1}$] at different levels.

Level (mb)	RH90	RH80C	RH80T	RH80TL
850	35	44	38	37
500	118	139	115	114
200	31	42	29	29

to that in RH80T (26) than in RH80 (9), RH80C (21), or RH80TL (29). Bias is better in RH80C than in RH80TL in only the 7–8-in. range, and it is better in RH80C than in RH80T in only the 1–2- and 7–8-in. ranges. The difference in bias values is small between RH80T and RH80TL, except that bias is worse in RH80TL (2) than in RH80T (1) for the 5–6-in. range. In summary, a comparison of threat sores and bias suggests that the performance of RH80T and RH80TL was better than RH80C.

c. *Condensational heating*

The structure of a tropical storm is primarily determined by the vertical distribution of heating. For an example of impact of differential heating in the vertical on storm circulation, see Mathur (1975). A comparison of the condensational heating rates at different levels between RH90 and a nudging experiment RH80T is shown in Fig. 2. Notice that the apportionment of the heating in two experiments is similar; the maximum in heating rate is largest in the midtroposphere, and it is somewhat smaller in the high troposphere than in the low troposphere. The horizontal structure of the heating rate is also similar in both experiments at all levels.

The vertical distribution of heating in the other nudging experiments (RH80C and RH80TL) was also similar to RH90. However, the maximum value at all levels differs by 2–4 K (6 h)$^{-1}$ in RH80T and RH80TL from RH90, and the maximum latent heating is considerably larger at all levels in RH80C than in RH90 (Table 3). The heating rates were much weaker at all levels in RH80 than in RH90; it is shown below that the predicted storm was much weaker in RH80 than in RH90. Because the condensation depends on the thermodynamic structure and vertical motion; the temperature, moisture, and vertical motion fields were much closer to the RH90 fields in the three nudging experiments than in RH80.

d. *Adjustment of winds*

The forecast 850-mb winds at 24 h over the storm area in five experiments are shown in Fig. 3. The maximum wind near the storm center at the initial time was 26 m s^{-1}. The storm intensifies into a hurricane by 24 h in RH90, and the maximum wind (42 m s^{-1}) occurs to the east of the center (Fig. 3a). It was noted previously that during the above 24-h period, the storm (Bob) also intensified into a hurricane in the real atmosphere. When the initial relative humidity is decreased in the storm area (experiment RH80), the storm does not intensify and the maximum wind is 21 m s^{-1} at 24 h (Fig. 3b).

With the nudging of the convective precipitation toward the RH90 rainfall (scheme 1, experiment RH80C), the rate of intensification becomes similar to RH90 (Fig. 3c). The maximum wind in RH90 and RH80C is nearly of the same strength, but there are two maximum in RH80C and only one in RH90. The circulation center in RH80C is located close to the RH90 center. The circulation center in RH80T and RH80TL is also located close to the RH90 center. The maximum wind is nearly of the same strength in RH90, RH80T, and RH80TL, and it is located to the east of the center in all three experiments. The minimum wind near the center is closer in magnitude to RH90 in RH80T than in RH80TL; the minimum wind is much stronger in RH80C than in RH90. The area occupied by the winds exceeding 20 m s^{-1} is somewhat smaller in RH80C than in RH90, RH80T, and RH80TL.

5. Concluding remarks

Recent studies, including those cited in section 1, have suggested that the circulation and rainfall errors in numerical forecasts models arise mainly due to the use of inadequate physical parameterization procedures or poor analysis. A few of these studies (e.g., Mathur et al. 1992) have also shown that the assimilation of rainfall data during initialization leads to an improvement in the initial divergence and moisture fields. Furthermore, use of a such improved initial state in a forecast model leads to the enhancement of the forecast rain and circulation even with the physical processes currently used in the models.

Our main effort in this paper was to develop and test rainfall nudging schemes that are more effective in improving model initial conditions and that are also computationally more efficient than the one used in Mathur et al. (1992). We designed three schemes. In the application of the reverse Kuo procedure for the nudging of rainfall, the convective precipitation is nudged in scheme 1, while the total precipitation is nudged in schemes 2 and 3. In addition, a method is included in scheme 3 for enhancing the rainfall at the nonconvective grid points where the forecast precipitation is weaker than the observed. Note that the reverse Kuo is not invoked at the nonconvective grid points. Numerical results presented in section 4 showed that scheme 3 performed the best and that scheme 2 was better than scheme 1. Thus, the nudging of the total rainfall in place of only the convective rain in the reverse procedure and the inclusion of a method to enhance the rainfall at the nonconvective grid points were beneficial.

It should be noted that we nudged only the rainfall, and the rainfall was adjusted toward the target (RH90)

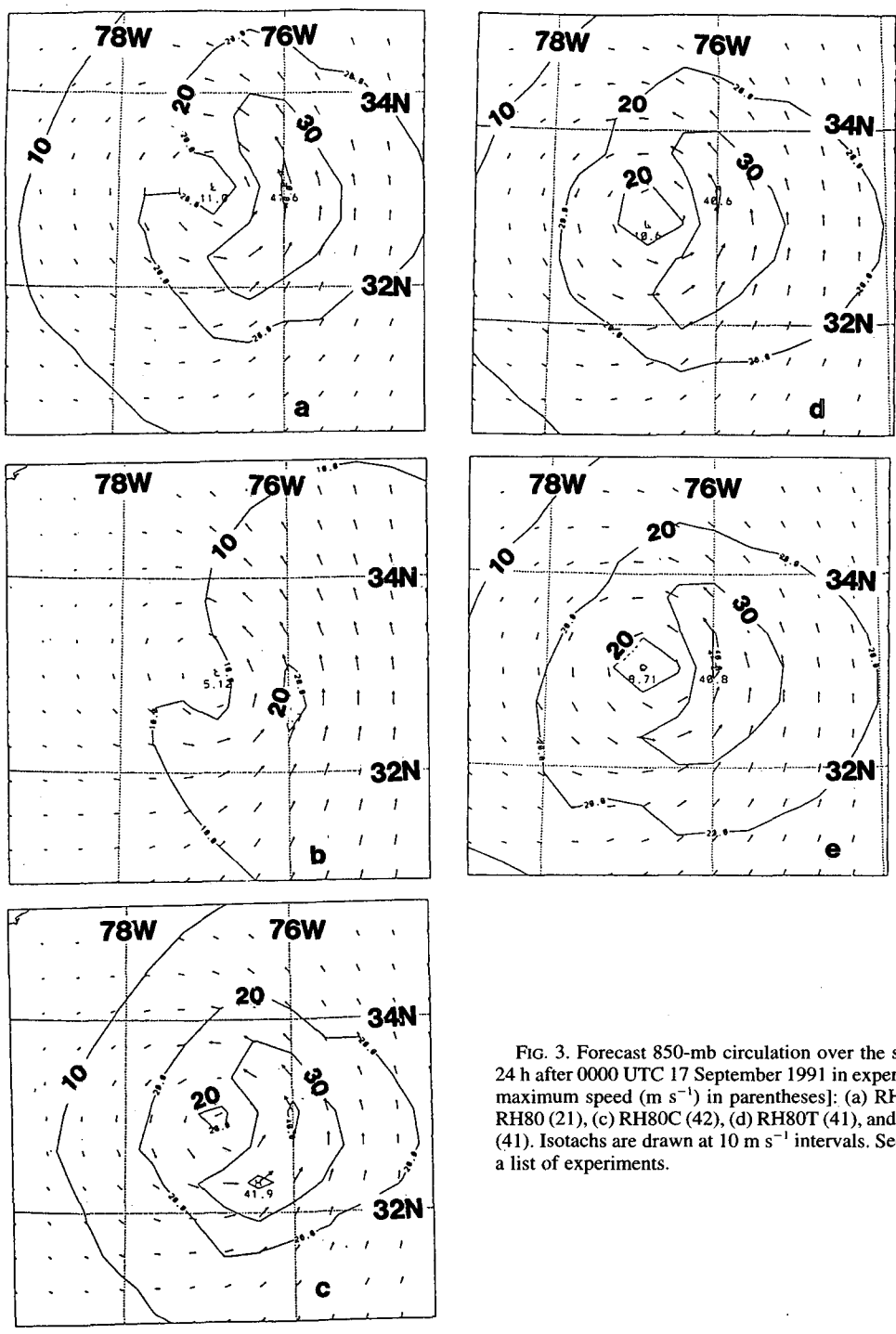

FIG. 3. Forecast 850-mb circulation over the storm area at 24 h after 0000 UTC 17 September 1991 in experiments [with maximum speed (m s^{-1}) in parentheses]: (a) RH90 (42), (b) RH80 (21), (c) RH80C (42), (d) RH80T (41), and (e) RH80TL (41). Isotachs are drawn at 10 m s^{-1} intervals. See Table 1 for a list of experiments.

rainfall in all three nudging experiments (section 4b, Fig. 1). Note also that the vertical and horizontal distribution of heating in the nudged experiments are similar to those in RH90 (section 4c, Fig. 2). It was pointed out in section 4c that the thermodynamic and vertical motion fields in the nudged experiments were also similar to those in RH90. Because the distribution of condensational heating largely determines a storm's structure, the circulation in the nudged experiments also became similar to that in RH90 (section 4d, Fig. 3). Thus, the assimilation of rainfall led to an improvement in the initial conditions.

The schemes proposed in this paper were used in a case where the rainfall was mainly associated with a tropical storm whose circulation extended vertically in the entire troposphere. On the other hand, the rainfall in the real atmosphere also occurs in disturbances that are shallow. As an example, the precipitation may occur in the region of a low-level trough. It should be also noted that we used model simulated rainfall data at 6-h intervals from the experiment RH90 in place of observations in this study, and these data were available over the entire domain of integration. Real data may be sparse and contain observational errors. A combination of idealized storm circulation and the data from a global analysis was used in the present study to define the initial state, and the impact of varying only the initial RH data in the storm area was investigated. The errors in the analysis may be in fields other than the relative humidity. Further tests utilizing only the analysis and observed rainfall data in the reverse schemes are required. In this regard we note that more frequent rainfall data over the entire Tropics from the satellite measurements are likely to become available soon at the NMC (section 1). When the above cited data become accessible, testing of these schemes over the entire tropical region using NMC's GDAS and MRF models will be carried out.

Acknowledgments. The author expresses his gratitude to two anonymous reviewers whose suggestions improved the quality of this paper.

REFERENCES

Adler, R. F., and A. J. Negri, 1988: A satellite infrared technique to estimate tropical convective and stratiform rainfall. *J. Appl. Meteor.*, **27,** 30–51.

Cheng, C.-P., and R. A. Houze, 1979: The distribution of convective and mesoscale precipitation in GATE radar echo patterns. *Mon. Wea. Rev.*, **107,** 1370–1381.

Donner, L. J., 1988: An initialization for cumulus convection in numerical weather prediction models. *Mon. Wea. Rev.*, **116,** 377–385.

——, and P. J. Rasch, 1989: Cumulus initialization in a global model for numerical weather prediction. *Mon. Wea. Rev.*, **117,** 2654–2671.

Kasahara, A., A. P. Mizzi, and L. J. Donner, 1992: Impact of cumulus initialization on the spinup of precipitation forecasts in the tropics. *Mon. Wea. Rev.*, **120,** 1360–1380.

Krishnamurti, T. N., H. S. Bedi, W. Heckley, and K. Ingles, 1988: Reduction of spinup time for evaporation and precipitation in a spectral model. *Mon. Wea. Rev.*, **116,** 907–920.

——, J. Xue, H. S. Bedi, K. Ingles, and D. Oosterhof, 1990: Physical initialization for numerical weather prediction over the Tropics. *Tellus,* **43AB,** 53–81.

Kuo, H. L., 1965: On formation and intensification of tropical cyclones through latent heat release by cumulus convection. *J. Atmos. Sci.*, **22,** 40–63.

Mathur, M. B., 1975: Development of banded structure in a numerically simulated hurricane. *J. Atmos. Sci.*, **32,** 512–522.

——, 1991: The National Meteorological Center's Quasi-Lagrangian Model for hurricane prediction. *Mon. Wea. Rev.*, **119,** 1419–1447.

——, and M. Baldwin, 1994: Development of vertical and slantwise convections in a ETA model's forecasts for the blizzard of 1993. *Proc. AMS Conf. on Numerical Weather Prediction,* Portland, OR, 108–109.

——, H. S. Bedi, T. N. Krishnamurti, M. Kanamitsu, and J. S. Woollen, 1992: Use of satellite-derived rainfall for improving tropical forecasts. *Mon. Wea. Rev.*, **120,** 2540–2560.

Manobianco, J., S. Koch, V. Mohan Karyampudi, and A. J. Negri, 1994: The impact of assimilating satellite-derived precipitation rates on numerical simulations of the ERICA IOP 4 cyclone. *Mon. Wea. Rev.*, **122,** 341–365.

Puri, K., and M. J. Miller, 1990: The use of satellite data in the specification of convective heating for diabatic initialization and moisture adjustment in numerical weather prediction models. *Mon. Wea. Rev.*, **118,** 67–93.